Attosecond transient absorption spectrum of argon at the $L_{2,3}$ edge

Andrew Chew,[1] Nicolas Douguet,[1] Coleman Cariker,[1] Jie Li,[1] Eva Lindroth,[2] Xiaoming Ren,[1] Yanchun Yin,[1]
Luca Argenti,[1] Wendell T. Hill III,[3,4,5] and Zenghu Chang[1,*]

[1]*CREOL and Department of Physics, University of Central Florida, Orlando, Florida 32816, USA*
[2]*Department of Physics, Stockholm University, 106 91 Stockholm, Sweden*
[3]*Joint Quantum Institute, University of Maryland, College Park, Maryland 20742, USA*
[4]*Institute for Physical Science and Technology, University of Maryland, College Park, Maryland 20742, USA*
[5]*Department of Physics, University of Maryland, College Park, Maryland 20742, USA*

Progress in high-harmonic generation has led to high-energy attosecond pulses with cutoff above the carbon $1s$ edge (283.8 eV). These pulses are essential to extend time-resolved spectroscopies to the water window in order to control electron dynamics in solvated organic species. Here we report a step towards this goal: the measurement, with subcycle time resolution, of the attosecond transient absorption spectrum of argon at the $2p^{-1}$ $L_{2,3}$ edge ($\sim$250 eV) in the presence of a short-wave infrared control pulse. The measurements, supported by theoretical simulations, demonstrate the concurrent role of Auger decay and tunnel ionization in the driven evolution of inner-valence holes of polyelectronic atoms.

Tabletop attosecond sources, based on the process of high-harmonic generation (HHG) [1], have made it possible to study, in a time-resolved way, the fast motion of electrons in gases [2] and in condensed matter [3,4]. Attosecond transient absorption spectroscopy (ATAS) [5,6], a pump-probe technique in which the spectrum of an attosecond extreme-ultraviolet or x-ray pulse transmitted through a sample is recorded as a function of the delay with respect to a second visible or infrared control pulse, in particular, has emerged as a promising candidate to study solvated species, since it does not require the detection of photoionization fragments. Attosecond transient absorption spectroscopy has already been applied to several atoms, such as krypton [5,7], argon [6,8], neon [9], and helium [10–15], as well as molecules, such as hydrogen [16] and oxygen [17] below or around 100 eV. Such comparatively small energy cutoffs constrain the duration of the attosecond pulses. Furthermore, absorption cross sections drop rapidly with light frequency until excitation of inner-valence and core electrons of large atoms such as carbon and titanium, which requires photons in the range of several hundred eV, becomes energetically possible.

Motivated by the desire to take advantage of the quadratic wavelength scaling of the harmonic cutoff [18], to extend the energy range of HHG, several groups have employed shortwave-infrared (SWIR) to midinfrared femtosecond sources which allowed for the generation of harmonic plateaus with cutoff beyond the $1s$ carbon edge [19–28]. This dramatic increase in the frequency bandwidth has led to a record in attosecond-pulse duration [29,30] as well as to the extension of femtosecond transient absorption to the core excitation of carbon-based molecules such as CF_4 Ref. [31] and 1,3-cyclohexadiene [32] and to inner-valence excitations of

third-period compounds such as SF_6 [31]. These experiments [31,32], however, focused on slow nuclear-rearrangement dynamics and hence did not rely on subcycle time resolution, which is a staple of attosecond spectroscopies.

In contrast, pump-probe experiments with subfemtosecond time-delay resolution and employing x-ray pulses with genuine attosecond duration are essential to access electron dynamics, such as charge migration [33,34], Auger decay [35,36], or the onset of symmetry-breaking processes, e.g., due to the Jahn-Teller effect [37–39], recently observed in Ref. [31].

Auger decay in atoms is an ideal benchmark for attosecond spectroscopies, as demonstrated for energies below 100 eV, in the case of krypton $M_{4,5}$-hole [35] and of helium doubly excited states [40]. In this energy region, many experiments have already highlighted the interplay between direct photoemission and Auger decay in photoelectron spectroscopies [41,42] and of resonant dispersive and absorptive response in ATAS [43,44]. Auger decay is also an attractive benchmark at much higher energies, close to the $1s$ carbon edge, where several atoms have inner-valence absorption edges, for example, the krypton M_3 edge, at 217 eV, and argon L_2 and L_3 edges, which lie, respectively, at 250.57 and 248.46 eV [45].

In this paper we present the ATAS measurement of the argon atom in the vicinity of the $2p^{-1}$ threshold, dressed by a strong SWIR pulse, polarized either parallel or orthogonal to the soft-x-ray probe, with subcycle time resolution and high-energy resolution. Our study resolves the dynamics of the autoionizing states converging to the $2p^{-1}$ $^2P^o_{3/2}$ threshold. Comparison with theoretical simulations for this polyelectronic system indicates that the measured resonant profiles, besides evident ac Stark shifts, bear the signature of concurrent Auger decay and tunnel ionization.

Figure 1(a) shows the experimental setup. A home-built optical parametric chirped pulse amplification source [46] generates 2-mJ carrier-envelope phase stable SWIR pulses,
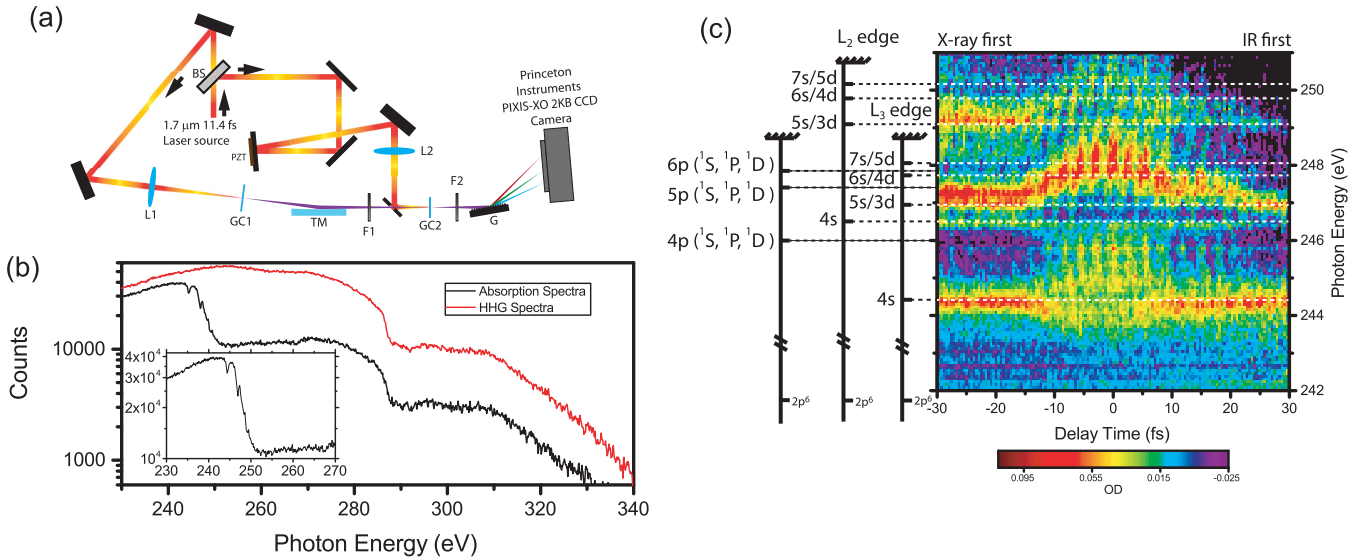
FIG. 1. (a) Experimental setup: BS, beam splitter; L1, CaF focusing lens ($f = 550$ mm); L2, CaF focusing lens ($f = 450$ mm); G, (1–6)-nm 2400 line/mm grating; TM, toroidal mirror; GC1, neon gas cell; GC2, argon gas cell; PZT, piezoelectric transducer; F1, 100-nm Sn filter; F2, 100-nm Al filter. (b) The HHG and argon absorption spectra as measured by the spectrometer. The inset gives an enlarged view of the argon absorption lines at the $L_{2,3}$ edge. (c) The ATAS spectra for parallel polarized x-ray and dressing SWIR pulses. The energy levels are marked accordingly. The dressing laser intensity is approximately 10^{13} W/cm^2.

with a central wavelength of 1.7 μm, a duration of $\sim$11 fs (two cycles), and at a 1-kHz repetition rate. The SWIR pulse is split into the HHG arm and the SWIR dressing arm. In the HHG arm, the SWIR is focused into a 1.5-mm-diam neon gas cell, where it reaches an estimated intensity of $\sim$4.7 $\times$ 10^{14} W/cm^2, to generate the attosecond pulse. A flat x-ray spectrum between 230 and 280 eV is observed, with no evidence of any harmonic peaks, which suggests that the x-ray generation is gated by the field amplitude of the driving pulse such that only one pulse in the train contributes to the spectrum at these energies. Indeed, harmonic peaks are observed at lower energies.

A 100-nm-thick tin filter at the end of the HHG arm blocks the residual SWIR pulse. The x-ray and time-delayed SWIR pulses are recombined via a hole-drilled mirror and focused onto the target argon gas. A 100-nm-thick aluminum filter reflects the SWIR component in the transmitted light field. The x-ray spectrum is recorded by a spectrometer, consisting of a 2400-line/mm grating which images the spectrum onto a CCD camera with an estimated resolution of $\sim$0.67 eV at 250 eV. Figure 1(b) shows the x-ray spectrum with and without the target gas, in the absence of any dressing pulse. Transmission through argon results in a pronounced drop of the spectral intensity in the region between 240 and 250 eV, where the two $2p^{-1}$ edges and the neutral metastable states they bind are located. The first terms of the bright autoionizing $2p_j^{-1}ns/nd$ series are clearly visible alongside the edge. The x-ray signal drop at 284 eV is due to carbon contamination of the optics.

Cao *et al.* [8] used ATAS to study how an external field imparts a finite linewidth to the $3p^{-1}n\ell$ bound states of argon. In the present case, the laser modifies the dynamics of states that already decay by emitting fast Auger electrons. The field-free Auger decay of $2p$-holes in argon has been the subject of several studies [47–50], as has the structure near the L edges, arising due to spectator electrons in the higher n states. The

$2p_{3/2}^{-1}4s$ state, for example, has a lifetime of 5.44 fs [49], which is well within the resolution of our experiment. Here, therefore, how the strong dressing field would affect the lifetime, position, and decay dynamics of these states can be studied.

Figure 1(c) shows the optical density (OD) of a typical ATAS, recorded in the presence of a relatively intense SWIR control pulse ($I_{\mathrm{SWIR}} \simeq 10^{13}$ W/cm^2), with polarization parallel to the x ray's, as a function of the x-ray SWIR time delay τ_d, in the interval -30 fs $\leqslant \tau_d \leqslant 30$ fs. The intensity of the dressing laser, which was inferred from the focusing geometry, has an uncertainty of a factor of 2. Throughout this paper, the time delay τ_d is negative when the x ray comes before the SWIR pulse and is recorded in steps of 0.423 fs, with an estimated jitter of 0.11 fs. To improve the signal-to-noise ratio in the spectra, at each delay time, the CCD camera signal is integrated for 60 s (i.e., 60 000 accumulated spectra). The transient optical density OD(ω, τ_d) is obtained from the spectrum of the x-ray light transmitted through the dressed target $I_{\mathrm{spectra}}(\omega, \tau_d)$ and the original HHG spectrum $I_0(\omega)$ as OD(ω, τ_d) = $\log_{10}(I_0/I_{\mathrm{spectra}})$. To better highlight the variation of the resonant absorption profiles, OD(ω, τ_d) $-$ OD$_{\mathrm{bg}}(\omega)$ is shown in Fig. 1(c), where OD$_{\mathrm{bg}}(\omega)$ is a smooth interpolation of the steep background profile.

Due to the large spin-orbit splitting ($\sim$2 eV) between the $^2P_{3/2}^o$ (L_3 edge) and $^2P_{1/2}^o$ (L_2 edge) Ar$^+$ $2p^{-1}$ ionic states, only one of the states that arise from the $^2P_{1/2}^o$ ion, the $2p^{-1}(^2P_{1/2}^o)4s$ resonance, located at $\sim$246.5 eV [49], lies below the L_3 edge. This state gives rise to a comparatively weak signal in the spectrum that does not appear to be affected much by the SWIR pulse. At large negative or positive delays, when the x-ray and the SWIR pulses do not overlap, the spectrum exhibits three main absorption peaks, due to the $2p_{3/2}^{-1}4s$ state, at $\sim$244.4 eV, the $2p_{3/2}^{-1}5s/3d$ group, at $\sim$246.9 eV, and the $2p_{1/2}^{-1}5s/3d$ group, at $\sim$249 eV, immediately above the L_3 threshold. Here
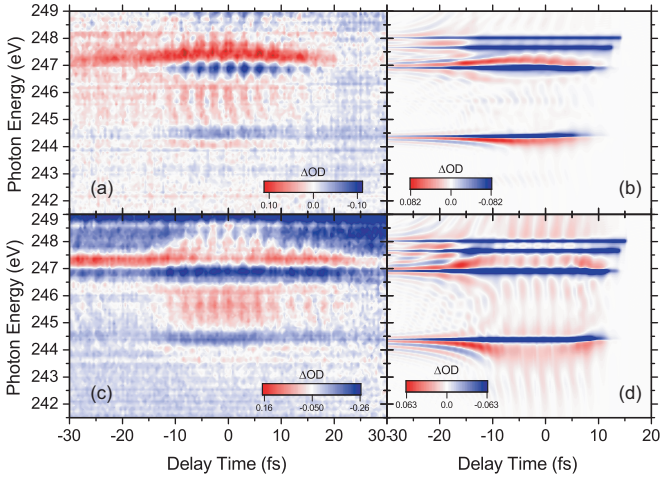
FIG. 2. (a) and (c) Measured and (b) and (d) computed ΔOD spectra for (a) and (b) $I_{\mathrm{SWIR}} = 10^{12}$ W/cm^2 and (c) and (d) $I_{\mathrm{SWIR}} = 10^{13}$ W/cm^2 for collinear x-ray and SWIR polarization.

the focus is on the states below the L_3 threshold. When the x-ray and SWIR pulses overlap, the spectrum changes in several ways: (i) The $2p_{3/2}^{-1}4s$ state and the $2p_{3/2}^{-1}5s/3d$ group exhibit a pronounced ac Stark shift, towards lower and higher energies, respectively; (ii) a broad signal between 245 and 246 eV appears, indicating the formation of light-induced states [51], at twice the SWIR frequency from the nearby resonances; (iii) the width of the $2p_{3/2}^{-1}5s/3d$ peak broadens as the states are shifted; (iv) the spectrum is modulated across the whole energy range by prominent, almost vertical interference fringes, with characteristic beating frequency twice as large as the SWIR signal's (time period of 5.67 fs). In Fig. 1(c) it is not possible to discern the characteristic hyperbolic fringes associated with the free-induction decay expected for isolated states [44,52,53]. However, all peaks do appear to be broader at negative time delays, when the SWIR pulse follows the x-ray pulse. The features observed in the transient absorption spectrum are due to the response of a single atom, instead of the macroscopic propagation through the dressed sample. This was ascertained by repeating the experiment using two different intensities of the dressing laser, with either collinear or orthogonal polarization with respect to the x-ray pulse, and at two gas pressures (40 and 80 torr).

To attribute the changes in the spectrum to the correct underlying physical process, time-dependent simulations were performed using a model that allows the disentangling of the individual couplings between autoionizing states from tunnel ionization. In particular, the prominent vertical fringes at twice the frequency of the dressing laser across a spectral region much larger than twice the SWIR photon energy suggest they have a nonperturbative origin. To improve the contrast in the spectrum without introducing an arbitrary background function, we plot the quantity $\Delta \mathrm{OD}(\omega, \tau_d) = \log_{10}[I_{\mathrm{X}}(\omega)/I_{\mathrm{spectrum}}(\omega, \tau_d)]$, where $I_{\mathrm{X}}(\omega)$ represents the spectrum transmitted through the target gas when the dressing pulse is entirely blocked.

Figure 2 compares the measured and the computed ΔOD spectra for collinear SWIR and x-ray polarization, at two different SWIR intensities $I_{\mathrm{SWIR}} = 10^{12}$ and

10^{13} W/cm^2. In the simulations, the time-dependent Schrödinger equation (TDSE) for the atom in the presence of the external fields is integrated numerically $|\Psi(t + dt)\rangle = U(t + dt, t)|\Psi(t)\rangle$ using a split-exponential propagator $U(t + dt, t) = \exp[-iH_{\mathrm{eff}}(t + dt/2)dt/2]\exp[-iH_I(t + dt/2)dt]\exp[-iH_{\mathrm{eff}}(t + dt/2)dt/2]$. Here $H_I(t) = -\vec{\mathcal{E}}(t)\cdot\vec{\mu}_{\mathrm{el}}$ is the field-atom interaction Hamiltonian in the dipole approximation, proportional to the total external electric field $\vec{\mathcal{E}}(t) = \vec{\mathcal{E}}_{\mathrm{X}}(t) + \vec{\mathcal{E}}_{\mathrm{SWIR}}(t; \tau_d)$, which accounts for the radiative coupling between bound and autoionizing states. The terms $[H_{\mathrm{eff}}(t)]_{ij} = \delta_{ij}[E_i - i\Gamma_i/2 - i\Gamma_i^{\mathrm{sf}}(t)]$ incorporate the field-free evolution of the states, through the time-independent state energy E_i and decaying width Γ_i, as well as the tunnel-ionization rate Γ_i^{sf}, which is estimated with the model of Perelomov *et al.* [54]. In the simulation, both pump and probe are Fourier-limited Gaussian pulses, with a full width half maximum duration of 200 as and 12 fs, respectively. At large positive delays, therefore, the theoretical spectrum coincides with the field-free absorption spectrum. In the experiment, on the other hand, the main SWIR pulse is accompanied by a pedestal, which is presumably the origin of the residual background signal at $\tau_d = 30$ fs in Fig. 2(c).

The transition dipole moments (TDMs) involving relevant bound and autoionizing states were computed using an updated version of Stock [55], a continuum-atomic-structure code based on the ATSP2K library [56,57]. First, the HF orbitals of the $2p^{-1}$ Ar$^+$ ion are computed. The $2p^{-1}$ and $3p^{-1}$ single-configuration Ar$^+$ ions are subsequently coupled to an electron with arbitrary angular momentum and radial part expressed in terms of a B-spline basis [58] to form the close-coupling channels for the neutral Ar atom that reproduce all the essential bound and autoionizing states in the system. The localized component of the $2p^{-1}n\ell$ autoionizing states is computed by diagonalizing the field-free nonrelativistic Hamiltonian in a basis that excludes the Auger-decay channels. Finally, the TDM between any two states is estimated by including only the transition between the corresponding localized components. To verify that these calculations are reliable, the dipole transition matrix elements were calculated independently using the MESA program [59] and the results were found to agree within 15%. The decaying rates of the autoionizing states used in the time propagation were identified with the experimental widths in [49]. Due to the large spin-orbit splitting of the $2p^{-1}$ hole, the states associated with the L_2 and L_3 edges do not mix significantly. Here we focus on the region below the L_3 edge and neglect the Ar$^+$ core splitting entirely. Although our oscillator strengths might therefore be overestimated, their relative strength should still be accurate.

The solution $\Psi(t, \tau_d)$ of the TDSE was computed to determine the time-dependent dipole moment $\mu_{el,z}(t, \tau_d) = \langle\Psi(t, \tau_d)|\hat{\mu}_{el}\cdot\hat{z}|\Psi(t, \tau_d)\rangle$, where $\hat{z}$ is the x-ray polarization axis. The transient single-atom optical density was finally evaluated as $\mathrm{OD}(\omega, \tau_d) = \frac{4\pi\omega}{c}\mathrm{Im}[\tilde{\mu}_{el,z}(\omega, \tau_d)/\tilde{\mathcal{E}}_{\mathrm{X}}(\omega)]$, where $\tilde{\mu}_{el,z}(\omega, \tau_d)$ and $\tilde{\mathcal{E}}_{\mathrm{X}}(\omega)$ are the Fourier transforms of the dipole moment and the x-ray electric field, respectively. Since I_{SWIR} in the experiment is not precisely known, we calibrate the corresponding I_{SWIR} in the simulation by comparing the theoretical predictions with the experimental spectra for the low-intensity collinear case [Fig. 2(a)]. Good agreement
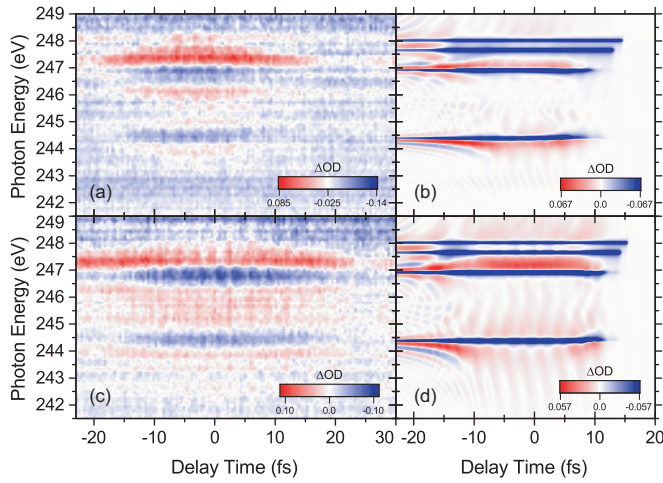
FIG. 3. Same as in Fig. 2 for orthogonal x-ray and SWIR polarization, with (a) and (b) $I_{SWIR} = 2.3 \times 10^{12}$ W/cm^2 and (c) and (d) 1.7×10^{13} W/cm^2.

was found for a theoretical I_{SWIR} twice as large as the nominal experimental one. This ratio was kept in all the calculations. All the intensities reported here refer to the values estimated in the experiment.

Both spectra in Figs. 2(a) and 2(b) exhibit a clear ac Stark shift of the $2p^{-1}_{3/2}4s$ and the $2p^{-1}_{3/2}5s/3d$ states as well as the gradual convergence to the field-free limit of the stronger $2p^{-1}_{3/2}5s/3d$ signal at large negative time delays, which is an indication of the resonance free-induction decay, even if the individual hyperbolic fringes do not have sufficient contrast to be visible in the experiment. The subcycle beating does not appear in the simulation if the photoionization of the autoionizing states to the continuum above the L_3 threshold are accounted for or if this process is modeled with a coupling between autoionizing and continuum states but continuum-continuum transitions are neglected. The model of Perelomov *et al.* [54] for the tunneling ionization rate, on the other hand, is able to qualitatively reproduce the vertical fringes.

At higher intensity, $I_{SWIR} = 10$ TW/cm^2, shown in Figs. 2(c) and 2(d), the most prominent effects are larger ac Stark shifts and the observation that the $2p^{-1}_{3/2}5s/3d$ complex traverses the more excited satellites, giving rise to the horizontal structure visible immediately below 248 eV. Finally, the experiment clearly indicates that the width of both the $2p^{-1}_{3/2}4s$

and the $2p^{-1}_{3/2}5s/3d$ states increases when the x-ray and the SWIR pulses overlap. In the case of the $2p^{-1}_{3/2}4s$, this increase is entirely attributable to the additional photoionization width imparted to the state by the field. The $2p^{-1}_{3/2}5s/3d$ complex, on the other hand, could also be split as a result of the radiative coupling to the nearby states. From the present measurements, it is difficult to discern which is the dominant broadening mechanism.

Figure 3 shows the same comparison as in Fig. 2, but for orthogonal x-ray and SWIR polarization. In this case, the coupling of the P^o states populated by the x ray to the S^e states is suppressed for geometrical reasons. Most of the features are similar to those already described in the collinear case, with one major difference: Whereas the ac Stark shift of the $2p^{-1}_{3/2}4s$ state is largely comparable to the one exhibited in the collinear case, the excursion of the $2p^{-1}_{3/2}5s/3d$ states is much smaller.

The results highlighted in this work suggest several possible lines of research in the strong-field ionization of metastable states: Does the polarization of inner-valence holes suppress tunneling of valence electrons? Does the correlation between an inner-valence hole and a satellite electron alter the polarizability of the parent ion? Is it possible to stabilize inner-valence holes with strong driving lasers? To answer these and related questions quantitatively for targets as complex as the argon atom will require us to refine the current measurements and pair them with TDSE simulations in spectral bases that explicitly accounts for spin-orbit coupling, which is beyond the scope of the present work.

In conclusion, we have demonstrated the measurement of the ATAS spectrum for autoionizing states next to the water window and with subcycle time resolution. These measurements open the way to extend attosecond time-resolved spectroscopies into the soft-x-ray energy range and to explore the interplay between strong-field ionization and many-electron dynamics such as Auger decay.

[1] F. Krausz and M. Ivanov, Rev. Mod. Phys. **81**, 163 (2009).

[2] M. Chini, K. Zhao, and Z. Chang, Nat. Photon. **8**, 178 (2014).

[3] F. Lépine, M. Y. Ivanov, and M. J. J. Vrakking, Nat. Photon. **8**, 195 (2014).

[4] M. Schultze, K. Ramasesha, C. Pemmaraju, S. Sato, D. Whitmore, A. Gandman, J. S. Prell, L. J. Borja, D. Prendergast, K. Yabana, D. M. Neumark, and S. R. Leone, Science **346**, 1348 (2014).

[5] E. Goulielmakis, Z.-H. Loh, A. Wirth, R. Santra, N. Rohringer, V. S. Yakovlev, S. Zherebtsov, T. Pfeifer, A. M. Azzeer, M. F.

Kling, S. R. Leone, and F. Krausz, Nature (London) **466**, 739 (2010).

[6] H. Wang, M. Chini, S. Chen, C.-H. Zhang, F. He, Y. Cheng, Y. Wu, U. Thumm, and Z. Chang, Phys. Rev. Lett. **105**, 143002 (2010).

[7] S. Pabst, A. Sytcheva, A. Moulet, A. Wirth, E. Goulielmakis, and R. Santra, Phys. Rev. A **86**, 063411 (2012).

[8] W. Cao, E. R. Warrick, D. M. Neumark, and S. R. Leone, New J. Phys. **18**, 013041 (2016).

[9] X. Wang, M. Chini, Y. Cheng, Y. Wu, X.-M. Tong, and Z. Chang, Phys. Rev. A **87**, 063413 (2013).

[10] S. Chen, M. J. Bell, A. R. Beck, H. Mashiko, M. Wu, A. N. Pfeiffer, M. B. Gaarde, D. M. Neumark, S. R. Leone, and K. J. Schafer, Phys. Rev. A **86**, 063408 (2012).

[11] M. Holler, F. Schapper, L. Gallmann, and U. Keller, Phys. Rev. Lett. **106**, 123601 (2011).

[12] M. Chini, B. Zhao, H. Wang, Y. Cheng, S. X. Hu, and Z. Chang, Phys. Rev. Lett. **109**, 073601 (2012).

[13] M. Chini, X. Wang, Y. Cheng, Y. Wu, D. Zhao, D. A. Telnov, S.-I. Chu, and Z. Chang, Sci. Rep. **3**, 1105 (2013).

[14] M. Reduzzi, J. Hummert, A. Dubrouil, F. Calegari, M. Nisoli, F. Frassetto, L. Poletto, S. Chen, M. Wu, M. B. Gaarde, K. Schafer, and G. Sansone, Phys. Rev. A **92**, 033408 (2015).

[15] C.-T. Liao, A. Sandhu, S. Camp, K. J. Schafer, and M. B. Gaarde, Phys. Rev. A **93**, 033405 (2016).

[16] Y. Cheng, M. Chini, X. Wang, A. González-Castrillo, A. Palacios, L. Argenti, F. Martín, and Z. Chang, Phys. Rev. A **94**, 023403 (2016).

[17] C.-T. Liao, X. Li, D. J. Haxton, T. N. Rescigno, R. R. Lucchese, C. W. McCurdy, and A. Sandhu, Phys. Rev. A **95**, 043427 (2017).

[18] B. Shan and Z. Chang, Phys. Rev. A **65**, 011804 (2001).

[19] X. Ren, J. Li, Y. Yin, K. Zhao, A. Chew, Y. Wang, S. Hu, Y. Cheng, E. Cunningham, Y. Wu, M. Chini, and Z. Chang, J. Opt. **20**, 023001 (2018).

[20] T. Popmintchev, M.-C. Chen, A. Bahabad, M. Gerrity, P. Sidorenko, O. Cohen, I. P. Christov, M. M. Murnane, and H. C. Kapteyn, Proc. Natl. Acad. Sci. USA **106**, 10516 (2009).

[21] H. Xiong, H. Xu, Y. Fu, J. Yao, B. Zeng, W. Chu, Y. Cheng, Z. Xu, E. J. Takahashi, K. Midorikawa, X. Liu, and J. Chen, Opt. Lett. **34**, 1747 (2009).

[22] N. Ishii, K. Kaneshima, K. Kitano, T. Kanai, S. Watanabe, and J. Itatani, Nat. Commun. **5**, 3331 (2014).

[23] A. S. Johnson, L. Miseikis, D. A. Wood, D. R. Austin, C. Brahms, S. Jarosch, C. S. Strüber, P. Ye, and J. P. Marangos, Struct. Dyn. **3**, 062603 (2016).

[24] S. M. Teichmann, F. Silva, S. L. Cousin, M. Hemmer, and J. Biegert, Nat. Commun. **7**, 11493 (2016).

[25] M.-C. Chen, P. Arpin, T. Popmintchev, M. Gerrity, B. Zhang, M. Seaberg, D. Popmintchev, M. M. Murnane, and H. C. Kapteyn, Phys. Rev. Lett. **105**, 173901 (2010).

[26] J. Li, X. Ren, Y. Yin, Y. Cheng, E. Cunningham, Y. Wu, and Z. Chang, Appl. Phys. Lett. **108**, 231102 (2016).

[27] G. J. Stein, P. D. Keathley, P. Krogen, H. Liang, J. P. Siqueira, C.-L. Chang, C.-J. Lai, K.-H. Hong, G. M. Laurent, and F. X. K. Kärtner, J. Phys. B **49**, 155601 (2016).

[28] T. Popmintchev, M.-C. Chen, D. Popmintchev, P. Arpin, S. Brown, S. Ališauskas, G. Andriukaitis, T. Balčiunas, O. D. Mücke, A. Pugzlys, A. Baltuška, B. Shim, S. E. Schrauth, A. Gaeta, C. Hernández-García, L. Plaja, A. Becker, A. Jaron-Becker, M. M. Murnane, and H. C. Kapteyn, Science **336**, 1287 (2012).

[29] J. Li, X. Ren, Y. Yin, K. Zhao, A. Chew, Y. Cheng, E. Cunningham, Y. Wang, S. Hu, Y. Wu, M. Chini, and Z. Chang, Nat. Commun. **8**, 186 (2017).

[30] T. Gaumnitz, A. Jain, Y. Pertot, M. Huppert, I. Jordan, F. Ardana-Lamas, and H. J. Wörner, Opt. Express **25**, 27506 (2017).

[31] Y. Pertot, C. Schmidt, M. Matthews, A. Chauvet, M. Huppert, V. Svoboda, A. von Conta, A. Tehlar, D. Baykusheva, J.-P. Wolf, and H. J. Wörner, Science **355**, 264 (2017).

[32] A. R. Attar, A. Bhattacherjee, C. D. Pemmaraju, K. Schnorr, K. D. Closser, D. Prendergast, and S. R. Leone, Science **356**, 54 (2017).

[33] F. Calegari, M. C. Castrovilli, M. Galli, E. Månsson, A. Trabattoni, D. Ayuso, S. D. Camillis, F. Frassetto, L. Poletto, A. Palacios, P. Decleva, J. Greenwood, F. Martin, and M. Nisoli, in *Proceedings of the International Conference on Ultrafast Phenomena* (Optical Society of America, Washington, DC, 2016), paper UM1A.1.

[34] F. Calegari, A. Trabattoni, A. Palacios, D. Ayuso, M. C. Castrovilli, J. B. Greenwood, P. Decleva, F. Martn, and M. Nisoli, J. Phys. B **49**, 142001 (2016).

[35] M. Drescher, M. Hentschel, R. Kienberger, M. Uiberacker, V. Yakovlev, A. Scrinzi, T. Westerwalbesloh, U. Kleineberg, U. Heinzmann, and F. Krausz, Nature (London) **419**, 803 (2002).

[36] T. Shimizu, T. Sekikawa, T. Kanai, S. Watanabe, and M. Itoh, Phys. Rev. Lett. **91**, 017401 (2003).

[37] I. B. Bersuker, Chem. Rev. **101**, 1067 (2001).

[38] D. R. Yarkony, Rev. Mod. Phys. **68**, 985 (1996).

[39] I. B. Bersuker, *The Jahn-Teller Effect*, 1st ed. (Cambridge University Press, Cambridge, 2006).

[40] S. Gilbertson, M. Chini, X. Feng, S. Khan, Y. Wu, and Z. Chang, Phys. Rev. Lett. **105**, 263003 (2010).

[41] M. Kotur, D. Guénot, Á. Jiménez-Galán, D. Kroon, E. W. Larsen, M. Louisy, S. Bengtsson, M. Miranda, J. Mauritsson, C. L. Arnold, S. E. Canton, M. Gisselbrecht, T. Carette, J. M. Dahlström, E. Lindroth, A. Maquet, L. Argenti, F. Martín, and A. L'Huillier, Nat. Commun. **7**, 10566 (2016).

[42] V. Gruson, L. Barreau, Á. Jiménez-Galan, F. Risoud, J. Caillat, A. Maquet, B. Carré, F. Lepetit, J.-F. Hergott, T. Ruchon, L. Argenti, R. Taïeb, F. Martín, and P. Salières, Science **354**, 734 (2016).

[43] C. Ott, A. Kaldun, P. Raith, K. Meyer, M. Laux, J. Evers, C. H. Keitel, C. H. Greene, and T. Pfeifer, Science **340**, 716 (2013).

[44] C. Ott, A. Kaldun, L. Argenti, P. Raith, K. Meyer, M. Laux, Y. Zhang, A. Blättermann, S. Hagstotz, T. Ding, R. Heck, J. Madroñero, F. Martín, and T. Pfeifer, Nature (London) **516**, 374 (2014).

[45] R. D. Deslattes, E. G. Kessler, P. Indelicato, L. de Billy, E. Lindroth, and J. Anton, Rev. Mod. Phys. **75**, 35 (2003).

[46] Y. Yin, J. Li, X. Ren, K. Zhao, Y. Wu, E. Cunningham, and Z. Chang, Opt. Lett. **41**, 1142 (2016).

[47] L. O. Werme, T. Bergmark, and K. Siegbahn, Phys. Scr. **8**, 149 (1973).

[48] L. O. Werme, T. Bergmark, and K. Siegbahn, Phys. Scr. **6**, 141 (1972).

[49] G. C. King, M. Tronc, F. H. Read, and R. C. Bradford, J. Phys. B **10**, 2479 (1977).

[50] P. A. Heimann, D. W. Lindle, T. A. Ferrett, S. H. Liu, L. J. Medhurst, M. N. Piancastelli, D. A. Shirley, U. Becker, H. G. Kerkhoff, B. Langer, D. Szostak, and R. Wehlitz, J. Phys. B **20**, 5005 (1987).

[51] M. B. Gaarde and K. J. Schafer, J. Phys. B **49**, 210501 (2016).

[52] M. Wu, S. Chen, S. Camp, K. J. Schafer, and M. B. Gaarde, J. Phys. B **49**, 062003 (2016).

[53] L. Argenti, A. Jiménez-Galán, C. Marante, C. Ott, T. Pfeifer, and F. Martín, Phys. Rev. A **91**, 061403 (2015).

[54] A. M. Perelomov, V. S. Popov, and M. V. Terent'ev, J. Expt. Theor. Phys. (U.S.S.R.) **50**, 1393 (1966) [Sov. Phys. JETP **23**, 924 (1966)].

[55] T. Carette, J. M. Dahlström, L. Argenti, and E. Lindroth, Phys. Rev. A **87**, 023420 (2013).

[56] C. Froese Fischer, Comput. Phys. Commun. **128**, 635 (2000).

[57] C. Froese Fischer, G. Tachiev, G. Gaigalas, and M. R. Godefroid, Comput. Phys. Commun. **176**, 559 (2007).

[58] H. Bachau, E. Cormier, P. Decleva, J. E. Hansen, and F. Martín, Rep. Prog. Phys. **64**, 1815 (2001).

[59] P. Saxe, B. H. Lengsfield, R. Martin, and M. Page, MESA (molecular electronic structure applications), University of California, 1990 (unpublished).